Aalborg Universitet

AALBORG UNIVERSITY
DENMARK

An approach to dynamic line rating state estimation at thermal steady state using direct and indirect measurements

Alvarez, David; Silva, Filipe Miguel Faria da; Mombello, Enrique E. ; Bak, Claus Leth; Rosero, Javier A.; Ólason, Daníel L.

An Approach to Dynamic Line Rating State Estimation at Thermal Steady State Using Direct and Indirect Measurements

David L. Alvarez[a,∗], F. Faria da Silva[b], Enrique E. Mombello[c], Claus Leth Bak[b], Javier A. Rosero[a], Daníel Leó Ólason[d]

[a]*Electrical Machines & Drives Group, EM&D, Universidad Nacional de Colombia, Carrera 30 No. 45 − 03, Edificio 453 Oficina 208, Bogotá, D.C, Colombia, 11001*
[b]*Department of Energy Technology, Aalborg University, Aalborg, Denmark*
[c]*Instituto de Energía Eléctrica, CONICET, Universidad Nacional de San Juan, San Juan, Argentina*
[d]*LANDSNET, Iceland*

Abstract

Dynamic line rating has emerged as a solution for reducing congestion in overhead lines, allowing the optimization of power systems assets. This technique is based on direct and/or indirect monitoring of conductor temperature. Different devices and methods have been developed to sense conductor temperature in critical spans. In this work, an algorithm based on WLS is proposed to estimate temperature in all ruling spans of an overhead line. This algorithm uses indirect measurements - i.e. weather reports and/or downscaling nowcasting models as inputs as well as direct measurements of mechanical tension, sag and/or conductor temperature. The algorithm has been tested using typical atmospheric conditions in Iceland along with an overhead line's real design, showing robustness, efficiency and the ability to minimize error in measurements.

Keywords: Dynamic Line Rating (DLR), Overhead Line (OHL), State Estimation (SE), Uncertainty propagation, Weighted Least Square (WLS)

1. Introduction

Overhead lines (OHLs) are facing new challenges in planning, operation and control. For instance, power system operators seek to push the operational limits [1] while maintaining high reliability levels. Under normal operating conditions the capacity of short and medium OHLs is commonly restricted by the minimum clearance between the conductor and the ground [2], which is defined by the sag of the catenary. To optimize OHLs capacity given this kind of restriction, Dynamic Line Rating (DLR) can be used [3]. With this technique a more realistic ampacity limit can be calculated. DLR sets dynamically ampacity limits using the actual atmospheric conditions, in opposition to the traditional approach (called Static Line Rating (SLR)), where the conductor's capacity is computed taking conservative or worst atmospheric conditions scenarios, that seldom occurs. The dynamic limit is commonly higher than the SLR limit; in reference [4] a higher ampacity (compared to the SLR limit) is measured 99% of the time when DLR is used. Consequently, a reduction in power congestion or bottlenecks and an increment of the margin of maneuver under contingencies is achieved when DLR is implemented. This is particularly beneficial when wind power is connected to the grid [5], because of the relation between wind speed, power generation and conductor ampacity. Indeed, given DLR advantages, applications for control, planning and operation of power systems are available in order to optimize these systems [6]. Examples of such applications are: inclusion of OHL temperature as a constraint to compute optimal power flows [7] or incorporating DLR into the scheduling [8, 9]. These applications can be added to the nowadays energy management systems [10].

Direct and indirect methods are used for DLR. Indirect methods are based on computing the conductor's temperature using data from weather stations close to the OHL and/or using atmospheric models coming from the area of influence of the line [11]. In contrast, direct methods take measurements directly from the OHL (frequency of vibration, mechanical tension, sag position, among others [3]) in order to

---

compute either the sag, the mechanical tension or the temperature over the conductor [10]. An additional option to increase reliability is the adoption of hybrid systems (direct and indirect measurements); for instance, in [12] both weather and tension measurements are used to monitor ampacity in OHLs spans. Although a set of DLR technologies is already available [13], a methodology to integrate both kinds of measurements to obtain a reliable overview of the entire line capacity is not available.

The conductor's resistance changes as a consequence of variations in temperature, which impacts the power flow [14] and the OHLs protections [15]. To model this, variations in temperature values along OHLs have been included in the line model in reference [16] by means of dividing the line into sections, based on gradients of temperature along the entire line. Given the relationship between resistance and temperature, the introduction of PMU measurements to estimate average conductor temperature along OHLs is proposed in reference [17]. Here the Weighted Least Square method (WLS) is applied. In a similar way, in [18] the average conductor temperature is computed at steady state and during thermal transients using only PMU, by means of linearizing the state estimation problem. In reference [19], an improved model based on PMU is presented. It considers the atmospheric conditions along the line route through π-equivalent circuits connected in series. These series represent sections of the OHL. Temperature is computed in the different sections.

In reference [20] the performance of PMU as DLR method is assessed, concluding that even though state estimation techniques are used, the error in the computed temperature is larger than acceptable margins as a result of both atmospheric changes along the line and error in measurements. To improve the conductor temperature estimation when applying PMU, different DLR methods can be used on the same OHL. For instance, in reference [21], the thermal resistivity coefficient is optimized through PMU and temperature measurements located in specific points of the line. This optimization is carried out as consequence of computing negative resistances when only PMUs are used. In reference [22], PMU and tension monitoring systems are used for DLR. This way, an overview of the line's temperature can be obtained using PMU and critical spans are directly monitored by the mechanical tension system.

As a consequence of the fact that critical span changes in time and space (which limits the OHL capacity), the number and location of spans to monitor have to be defined. In reference [23] a heuristic methodology to identify critical spans based on computing conductor temperature in each span is proposed. In that study the span temperature is estimated using data from historical weather reports and climate models. In reference [24] a similar methodology is developed considering the clearances to ground, instead of the conductor temperature. Although methodologies to identify critical spans tend to use optimization algorithms, a risk level is assumed in the spans that are not being monitored. In consequence, it is desirable to know or at least to estimate the state of all spans in an economical and reliable way. An option to estimate weather conditions along the line is to interpolate atmospheric parameters in space (nowcasting) using meteorological models and/or a set of atmospheric measurements [25] taken close to the influence area of the OHL. Thus, with a set of monitoring stations covering critical spans and nowcasting along the OHL, a reliable overview of the entire conductor temperature can be achieved. However, even assuming that a complete conductor capacity monitoring system is available in each span, errors in the computing of conductor temperature as a result of uncertainties in both measurements and conductor parameters are presented [26]. Moreover, error is higher for low currents [27]. This is common in OHLs that operate at low capacities in order to guarantee the reliability criteria $N-1$. Consequently, various efforts have been carried out in order to quantify the impact of different kinds of errors over temperature estimation. In reference [27] a methodology to analyze the influence of conductor temperature measurement errors over the computed ampacity is presented. In reference [28] an estimation algorithm based on the Monte Carlo method is developed. It considers uncertainty in the heat transfer model and in atmospheric measurements. A similar analysis is presented in [29], by applying affine arithmetic in order to identify critical spans and to find out the corresponding temperature.

The previous state estimation algorithms only apply to direct [17, 18] or indirect measurements [28, 29], but not to hybrid systems. Therefore, to minimize errors in temperature estimation of all spans of an OHL, this work proposes a state estimation (SE) algorithm based on WLS. In this algorithm the elements of the Jacobian matrix, the elements of the measurement weight matrix and the measurement functions are presented in a novel way. It uses the available direct and indirect measurements and adds the advantage of including redundant measurements as numerical weather prediction (NWP) and downscaling atmospheric nowcasting models, thus increasing reliability. This is important, since reliability is affected when DLR devices are included in the system [30]. In Figure 1 the SE problem is shown. It is expected that the measurements (z) and the OHL parameters contain errors (e). The SE issue is stated with the objective of obtaining the best estimated both of the electrical RLC parameters and of the temperature (T_S) in each ruling span of the OHL. This paper is organized as follows: the different methods to compute

2

the average conductor temperature are discussed in section 2. In section 3, the proposed methodology is presented and the algorithm to minimize errors in temperature estimation along the entire OHL is developed. Finally, simulation results obtained from testing this algorithm under typical atmospheric conditions are presented in section 4. The simulations are based on real OHL data.
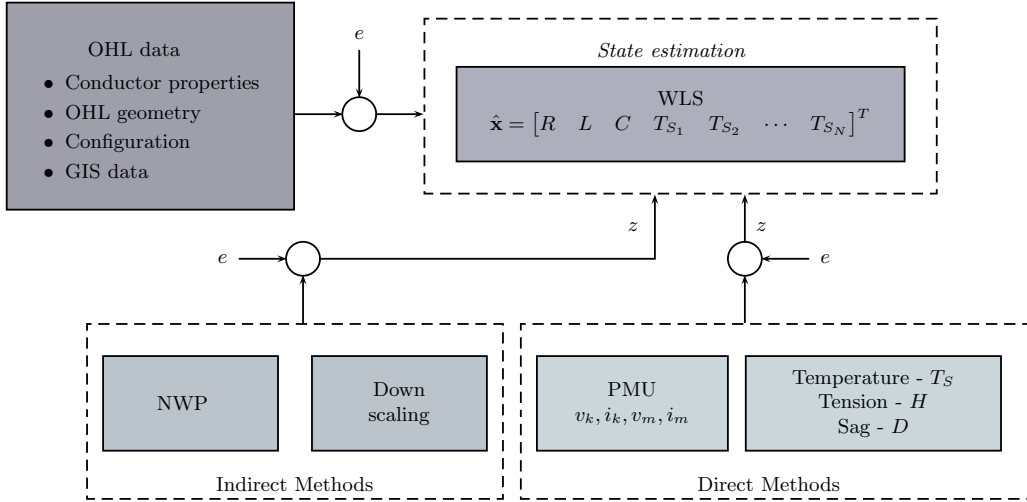

Figure 1: Dynamic Line Rating estimation using WLS, an overview using direct and indirect measurements

2. Review of Dynamic Line Rating Methods

In this section, mathematical models and approximations employed to calculate the temperature of OHL conductors using direct and indirect measurements are presented. These expressions are used as measurement functions in the formulation of the proposed SE algorithm. This algorithm estimates the conductor temperature in steady state, which occurs during normal operating conditions. In steady state, it is assumed that the current intensity and environmental conditions are constant during a certain period of time, typically one hour [10]. Thus, the thermal transient term can be neglected. To use steady state analysis, temperature is estimated at the moment that the conductor reaches the thermal equilibrium, which is a conservative assumption. With this temperature value, the maximum conductor ampacity can be calculated. However, if a short-term overload occurs, the state estimation is affected, being necessary to do a continued estimation. The possibility of including thermal transients in a dynamic state estimation problem will be object of future research.

2.1. Indirect measurements - Heat transfer equilibrium

Indirect method refers to the use of atmospheric conditions to compute the conductor temperature. This method is based on the heat transfer between the conductor and the environment as a consequence of heat losses and heat gains. Any change in the thermal conditions produces a thermal transient until the conductor reaches the thermal equilibrium. This equilibrium can be described by the heat balance

$$Q_J + Q_S = Q_C + Q_R \tag{1}$$

where Q_J and Q_S are the heat gains by Joule effect and solar radiation, and Q_C and Q_R are the heat losses by cooling and radiation. The inputs of (1) are the wind speed and direction, the solar radiation, the ambient temperature and the current intensity. As a consequence of wind variations in time and space, it is recommended to use average values [31] as input for the heat balance equation. These average values are commonly available in weather reports. Additionally, a set of conductor parameters must be included as inputs. They increase error in the computing of temperature if not correctly chosen. For instance, in [26] a linear statistical model is proposed with the aim of improving accuracy, which can be influenced by errors in the physical parameters and by the approximations used to compute both heat gains and losses in (1). In this paper the CIGRE model [32] is used as measurement function.

3

2.2. Tension measurements - State equation

To relate changes in temperature with variations of tension in OHL conductors the state change equation can be used [33]. In this work, the tension is assumed equal in each tensioning section of the OHL and thus the ruling span approximation is used [34]. Because of conductor creep has low impact in the sag calculation [35], this is considered as a source of error in estimation. Therefrom, only the linear thermal and elastic elongation models are considered in the state change equation (2).

$$\frac{EA\left(R_s m_c g\right)^2}{24} = H_S{}^2 \left[H_S - H_{T_{ref}} + \frac{EA\left(R_s m_c g\right)^2}{24 H_{T_{ref}}{}^2} + EA\varepsilon_t\left(T_S - T_{ref}\right) \right] \tag{2}$$

In this equation (2) E is the modulus of elasticity, A is the conductor cross section, H and $H_{T_{ref}}$ are the horizontal tension at temperature T_S and at reference temperature T_{ref}, R_s is the ruling span length, m_c is the conductor mass per unit length, g is the gravitational acceleration and ε_t is the coefficient of thermal expansion.

2.3. Sag measurements - Catenary equation

Sag measurements are used to obtain the clearance between the OHL conductor and the ground in order to assess the OHL thermal capacity. Another way to calculate the OHL rating is to compute the mechanical tension with sag measurements and use these values to compute the conductor's temperature by using the state change equation. This methodology is proposed in [36] using the parabolic approximation. However, for large spans the catenary solution is used, which relates sag (D) with tension (H) through (3), where s is the span length.

$$D = \frac{H}{m_c g}\left[\cosh\left(\frac{m_c g s}{2H}\right) - 1\right] \tag{3}$$

To express mechanical tension as a function of sag, the equation (3) is expanded as a Taylor series in (4), where the first term is equal to the parabolic approximation.

$$D = \frac{s^2 m_c g}{8\,H} + \frac{s^4\left(m_c g\right)^3}{384\,H^3} + \frac{s^6\left(m_c g\right)^5}{46080\,H^5} + \cdots \tag{4}$$

In this work, the first and second term of the series (4) are used to compute tension as a function of sag, obtaining the polynomial form (5). This expression has the form of the polynomial of degree three $ax^3 + bx^2 + cx + d = 0$, where $a = D$, $b = -s^2 m_c g/8$, $c = 0$ and $d = -s^4\left(m_c g\right)^3/384$.

$$H^3 D - \frac{s^2 m_c g\,H^2}{8} - \frac{s^4\left(m_c g\right)^3}{384} \approx 0 \tag{5}$$

The solution to the polynomial (5) is (6)

$$H\left(D\right) = \sqrt[3]{q + \sqrt{q^2 + \left(r - p^2\right)^3}} + \sqrt[3]{q - \sqrt{q^2 + \left(r - p^2\right)^3}} + p \tag{6}$$

where $p = -\frac{b}{3a}$, $q = p^3 + \frac{bc - 3ad}{6a^2}$ and $r = \frac{c}{3a}$. This equation expresses analytically the tension (H) in function of the sag (D), allowing to compute the conductor temperature using sag measurements.

To compare the performance between the parabolic approximation (first term) and the use of the two first terms of the catenary series expansion proposed to compute sag, the error between the exact solution (3) and these approximation is contrasted under common values of span length and tension, supposing a $m_c = 1.294$ [kg/m]. Figure 2a shows the error (e) between the catenary function and the parabolic approximation. Similarly, Figure 2b shows the error between the catenary function and the approximation using the first two terms of the series. To use the first two terms of the catenary series expansion results in an error inferior to 0.05 %. When the parabolic approximation is used, an error around 3 % is obtained for long sags and low tensions. Consequently, a high accuracy is reached when only the first two terms of the catenary series expansion are considered, since it allows to analytically express the tension as a function of sag with an error lower than 0.05 %.
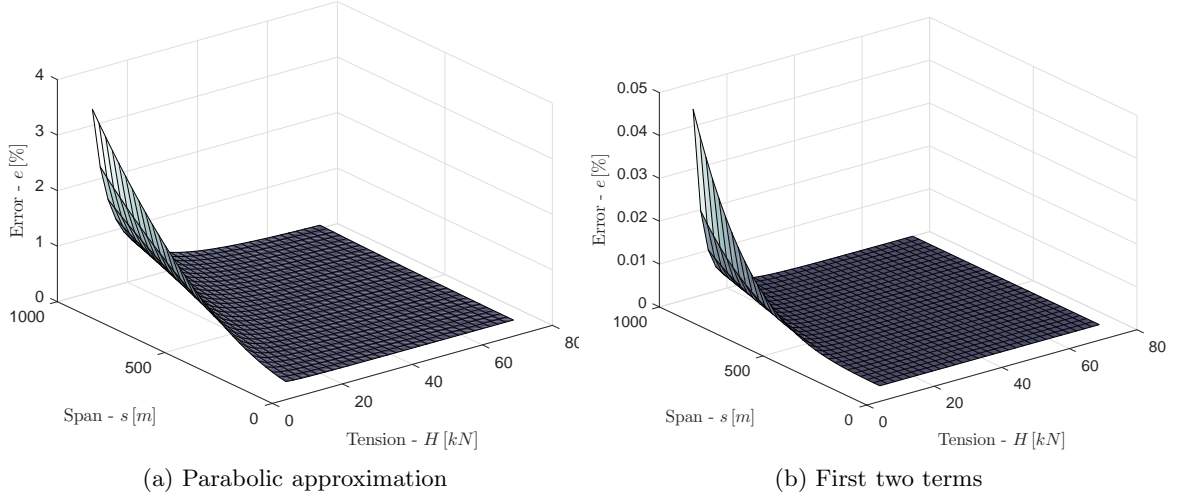
(a) Parabolic approximation   (b) First two terms

Figure 2: Error in the computing of sag using Taylor series expansion of cosh

2.4. Temperature measurements

The temperature of the conductor can be measured directly with sensors installed on the OHL. However, in spite of directly sensing temperature, it is necessary to install a set of measurement devices along the span because of the fact that temperature changes [37]. This as a consequence of the wind behavior, the presence of clouds, close objects, among other factors which affects heat transfer. Consequently, the conductor temperature is assumed as the average of the set of measurements.

2.5. Synchrophasor measurements

The computing of conductor ampacity with PMU is based on indirect measurements of temperature. This method takes the synchronized values of voltage (v_k, v_m) and current (i_k, i_m) at the ends of the OHL to calculate its impedance. Thus, using the resistive part of impedance the average conductor temperature along the OHL can be calculated, provided that the relationship between resistance and temperature is known. When a π line model is used, the impedance $(Z = R(T_S) + jX_L)$ and admittance $(Y = jY_C)$ are related to voltages and currents by means of (7) and (8).

$$i_k = Y\left(\frac{Z \cdot Y}{4} + 1\right)v_m - \left(\frac{Z \cdot Y}{2} + 1\right)i_m \tag{7}$$

$$v_k = \left(\frac{Z \cdot Y}{2} + 1\right)v_m - Z \cdot i_m \tag{8}$$

3. Proposed method for DLR State Estimation (SE)

Both economic and reliability considerations must be taken into account for implementing DLR systems. For lowering costs, a solution is to use weather nowcasting and PMU when available, and in order to increase reliability, direct measurements on critical spans are necessary. Considering these aspects, a new algorithm to estimate conductor temperature in each ruling span of an OHL is proposed in this work using PMU, weather nowcasting and direct measurements.

3.1. Definition of the estimation problem

In this proposed method, the definition of the SE problem is based on the measurement model functions $\mathbf{h}(\mathbf{z}, \mathbf{x})$ (9), which model the errors ($\mathbf{e}$) in a set of measurements $\mathbf{z}$ (10) by means of the state vector ($\mathbf{x}$). In other words, the measurement functions compute the error between measurements and state variables using known relationships. If the values of either temperature, tension, or sag along the entire OHL are known, it is possible to compute the thermal state of the line [6]. Therefore, both the temperature in each ruling span (T_{S_n}) and the RLC parameters of the equivalent OHL π circuit were chosen as state variables (11) in this paper.

$$0 = \mathbf{h}(\mathbf{z}, \mathbf{x}) + \mathbf{e} \tag{9}$$

5

$$\mathbf{z} = \begin{bmatrix} \mathrm{Re}\,(v_k) & \mathrm{Im}\,(v_k) & \mathrm{Re}\,(i_k) & \mathrm{Im}\,(i_k) & \mathrm{Re}\,(v_m) & \mathrm{Im}\,(v_m) & \mathrm{Re}\,(i_m) & \mathrm{Im}\,(i_m) & \mathbf{z}_W & \mathbf{z}_{T_S} & \mathbf{z}_H & \mathbf{z}_D \end{bmatrix} \tag{10}$$

$$\mathbf{x} = \begin{bmatrix} R & L & C & T_{S_1} & T_{S_2} & \cdots & T_{S_N} \end{bmatrix}^T \tag{11}$$

The reason for selecting the conductor temperature as state variable is because of the direct relationship between losses, resistance and temperature. It allows the integration of all DLR measurements (PMU, weather, temperature, tension and sag). These relationships are described by (12) and (13)

$$\left| i_k - \frac{v_k Y}{2} \right|^2 R = \left| \frac{v_m Y}{2} - i_m \right|^2 \sum_{n=1}^{N} R_n \,(T_{S_n}) \tag{12}$$

$$R = \sum_{n=1}^{N} R_n \,(T_{S_n}) \tag{13}$$

where R_n is the resistance and T_{S_n} is the temperature of the conductor in the ruling span n.

The elements of the measurement vector $\mathbf{z}$ (10) are:

1. v and i are the complex values of voltage and current at ends (k, m) of the OHL, measured at the same time.

2. The vectors $\mathbf{z}_W$ (14) are the set of atmospheric parameters $\mathbf{w} = \begin{bmatrix} T_a & S & \vartheta & \delta \end{bmatrix}$ in each ruling span. T_a is the ambient temperature, S is the solar radiation, ϑ is the wind speed and δ is the attack angle of the wind. N is the number of ruling spans.

$$\mathbf{z}_W = \begin{bmatrix} \mathbf{w}_1 & \mathbf{w}_2 & \cdots & \mathbf{w}_N \end{bmatrix} \tag{14}$$

3. The vector $\mathbf{z}_{T_S}$ (15) is the set of temperature measurements over the conductor. These measurements are located in specifics ruling spans $(\mathbf{F}_{T_S})$ along the OHL. N_T is the number of measurements.

$$\mathbf{z}_{T_S} = \begin{bmatrix} T_{S_1} & T_{S_2} & \cdots & T_{S_n} & \cdots & T_{S_{N_T}} \end{bmatrix} \; n \in \mathbf{F}_{T_S} \tag{15}$$

4. The vector $\mathbf{z}_H$ (16) is the set of tension measurements available on the OHL. N_H is the number of tension devices located on specific ruling spans $(\mathbf{F}_H)$.

$$\mathbf{z}_H = \begin{bmatrix} H_1 & H_2 & \cdots & H_n & \cdots & H_{N_H} \end{bmatrix} \; n \in \mathbf{F}_H \tag{16}$$

5. The vector $\mathbf{z}_D$ (17) is the set of sag measurements available on the OHL located in $(\mathbf{F}_D)$. N_D is the number of devices that are sensing the sag.

$$\mathbf{z}_D = \begin{bmatrix} D_1 & D_2 & \cdots & D_n & \cdots & D_{N_D} \end{bmatrix} \; n \in \mathbf{F}_D \tag{17}$$

Finally, with the state variables $(\mathbf{x})$ defined and with the DLR measurements functions addressed in section 2, the SE is stated as follows: if $\hat{\mathbf{x}}$ is assumed to be the best estimates of $\mathbf{x}$, a residual vector $\boldsymbol{\varepsilon}$ (18) is obtained to evaluate the measurement functions $\mathbf{h}(\mathbf{z}, \hat{\mathbf{x}})$. These functions are formed as in (19) and are described in the AppendixA.

$$\boldsymbol{\varepsilon} = \mathbf{h}\,(\mathbf{z}, \hat{\mathbf{x}}) \tag{18}$$

$$\begin{aligned} \mathbf{h}\,(\mathbf{z}, \mathbf{x}) = \big[\mathrm{Re}\,(h_v\,(\mathbf{z}, \mathbf{x})) & \quad \mathrm{Im}\,(h_v\,(\mathbf{z}, \mathbf{x})) \quad \mathrm{Re}\,(h_i\,(\mathbf{z}, \mathbf{x})) \quad \mathrm{Im}\,(h_i\,(\mathbf{z}, \mathbf{x})) \quad \dots \\ & h_R\,(\mathbf{z}, \mathbf{x}) \quad h_P\,(\mathbf{z}, \mathbf{x}) \quad \mathbf{h}_Q\,(\mathbf{z}, \mathbf{x}) \quad \mathbf{h}_T\,(\mathbf{z}, \mathbf{x}) \quad \mathbf{h}_H\,(\mathbf{z}, \mathbf{x}) \quad \mathbf{h}_D\,(\mathbf{z}, \mathbf{x}) \big]^T \end{aligned} \tag{19}$$

3.2. Weighted Least Squares - WLS

To compute the best estimate of the temperature in each ruling span, the most common error norm is applied in this paper: Least Square Error norm or Squared Euclidian norm [38]. Thus, the least square estimated is the vector $\hat{\mathbf{x}}$ that minimizes the norm $|\boldsymbol{\varepsilon}|^2$ (20) (also called measurement residual $\mathbf{J}\,(\mathbf{x})$)

$$|\boldsymbol{\varepsilon}|^2 = \sum_{n=1}^{N_m} w_n h_n(\mathbf{z}, \hat{\mathbf{x}})^2 = [\mathbf{h}(\mathbf{z}, \hat{\mathbf{x}})]^T \, [\mathbf{W}] \, [\mathbf{h}(\mathbf{z}, \hat{\mathbf{x}})] \tag{20}$$

where N_m is the number of measurement functions and equal to the size of vector (19). $\mathbf{W}$ is a diagonal matrix whose elements are the measurement weights $w_n{}^2$ which are calculated using the measurement's

standard deviation. Equations derived to compute w_n are in the AppendixB. Finally, the cost function to obtain the best estimated is given by (21).

$$\min_x \mathbf{J}\left(\mathbf{x}\right) = \left[\mathbf{h}(\mathbf{z}, \hat{\mathbf{x}})\right]^T \left[\mathbf{W}\right] \left[\mathbf{h}(\mathbf{z}, \hat{\mathbf{x}})\right] \tag{21}$$

The minimum value of $\mathbf{J}\left(\mathbf{x}\right)$ is found when $\partial \mathbf{J}\left(\mathbf{x}\right)/\partial \mathbf{x} = 0$, or the gradient $\nabla_x \mathbf{J}\left(\mathbf{x}\right) = 0$ [39], as shown in (22),

$$\nabla_x \mathbf{J}\left(\mathbf{x}\right) = \left[\mathbf{H}\right]^T \left[\mathbf{W}\right] \left[\mathbf{h}(\mathbf{z}, \hat{\mathbf{x}})\right] \tag{22}$$

where $\mathbf{H}$ is the Jacobian matrix, defined as $\mathbf{H} = \partial \mathbf{h}(\mathbf{z}, \mathbf{x})/\partial \mathbf{x}$. The proposed $\mathbf{H}$ matrix has the form of (23) assuming that all kind of DLR measurements are available. The partial derivatives that form $\mathbf{H}$ are in AppendixC.

$$\mathbf{H} = \begin{bmatrix} \dfrac{\partial \operatorname{Re}\left(h_v\left(\mathbf{z}, \mathbf{x}\right)\right)}{\partial R} & \dfrac{\partial \operatorname{Re}\left(h_v\left(\mathbf{z}, \mathbf{x}\right)\right)}{\partial X_L} & \dfrac{\partial \operatorname{Re}\left(h_v\left(\mathbf{z}, \mathbf{x}\right)\right)}{\partial Y_C} & 0 \\[2mm] \dfrac{\partial \operatorname{Im}\left(h_v\left(\mathbf{z}, \mathbf{x}\right)\right)}{\partial R} & \dfrac{\partial \operatorname{Im}\left(h_v\left(\mathbf{z}, \mathbf{x}\right)\right)}{\partial X_L} & \dfrac{\partial \operatorname{Im}\left(h_v\left(\mathbf{z}, \mathbf{x}\right)\right)}{\partial Y_C} & 0 \\[2mm] \dfrac{\partial \operatorname{Re}\left(h_i\left(\mathbf{z}, \mathbf{x}\right)\right)}{\partial R} & \dfrac{\partial \operatorname{Re}\left(h_i\left(\mathbf{z}, \mathbf{x}\right)\right)}{\partial X_L} & \dfrac{\partial \operatorname{Re}\left(h_i\left(\mathbf{z}, \mathbf{x}\right)\right)}{\partial Y_C} & 0 \\[2mm] \dfrac{\partial \operatorname{Im}\left(h_i\left(\mathbf{z}, \mathbf{x}\right)\right)}{\partial R} & \dfrac{\partial \operatorname{Im}\left(h_i\left(\mathbf{z}, \mathbf{x}\right)\right)}{\partial X_L} & \dfrac{\partial \operatorname{Im}\left(h_i\left(\mathbf{z}, \mathbf{x}\right)\right)}{\partial Y_C} & 0 \\[2mm] \dfrac{\partial h_R\left(\mathbf{z}, \mathbf{x}\right)}{\partial R} & 0 & 0 & \dfrac{\partial h_R\left(\mathbf{z}, \mathbf{x}\right)}{\partial \mathbf{T_S}} \\[2mm] \dfrac{\partial h_E\left(\mathbf{z}, \mathbf{x}\right)}{\partial R} & 0 & \dfrac{\partial h_E\left(\mathbf{z}, \mathbf{x}\right)}{\partial Y_C} & \dfrac{\partial h_E\left(\mathbf{z}, \mathbf{x}\right)}{\partial \mathbf{T_S}} \\[2mm] 0 & 0 & \dfrac{\partial \mathbf{h_P}\left(\mathbf{z}, \mathbf{x}\right)}{\partial Y_C} & \dfrac{\partial \mathbf{h_P}\left(\mathbf{z}, \mathbf{x}\right)}{\partial \mathbf{T_S}} \\[2mm] 0 & 0 & 0 & \dfrac{\partial \mathbf{h_{T_S}}\left(\mathbf{z}, \mathbf{x}\right)}{\partial \mathbf{T_S}} \\[2mm] 0 & 0 & 0 & \dfrac{\partial \mathbf{h_H}\left(\mathbf{z}, \mathbf{x}\right)}{\partial \mathbf{T_S}} \\[2mm] 0 & 0 & 0 & \dfrac{\partial \mathbf{h_D}\left(\mathbf{z}, \mathbf{x}\right)}{\partial \mathbf{T_S}} \end{bmatrix} \tag{23}$$

As the relationships between the states $\mathbf{x}$ and measurement functions $\mathbf{h}(\mathbf{z}, \mathbf{x})$ are nonlinear in almost all cases, an iterative process is necessary in order to estimate $\hat{\mathbf{x}}$ numerically. In this work the iterative Newton's method is used to compute the states $\hat{\mathbf{x}}_{\mathbf{k}} = \hat{\mathbf{x}}_{\mathbf{k-1}} - \Delta\hat{\mathbf{x}}$, where $\Delta\hat{\mathbf{x}}$ is defined by (24).

$$\Delta\hat{\mathbf{x}} = \left[\left[\mathbf{H}\right]^T \left[\mathbf{W}\right] \left[\mathbf{H}\right]\right]^{-1} \left[\mathbf{H}\right]^T \left[\mathbf{W}\right] \left[\mathbf{h}(\mathbf{z}, \hat{\mathbf{x}})\right] \tag{24}$$

The number of state variables is $N_s = 3 + N$ (size of the vector (11)) and the number of measurement functions is $N_m = 6 + N + N_T + N_H + N_D$. Therefore, provided that at least PMU measurements and weather nowcasting are available the system is overdetermined, because $N_m > N_s$. To summarize, algorithm 1 shows the procedure developed to estimate the conductor temperature in each ruling span and the OHL's RLC parameters. During the evaluation of the algorithm non-convergence was detected when the initial guess of temperature was far away of the true temperature, and when the direct measurements had opposite sign (consider bad data). This induces to either the computing of negative tension forces, which generate complex residuals, or to estimating temperatures below of the absolute zero. Two **IF** statements are included into the algorithm to avoid these negative outcomes. However, the identification of other possible conditions of non-convergence will be subject of future research.

4. Case Study

Due to the fact that methods to minimize error in conductor temperature computing along OHLs using direct and indirect measurements are not available in literature, the proposed algorithm could not be compared to similar ones. Thus, in order to evaluate the performance of the algorithm, it was implemented in Matlab® and tested with the data of a real OHL under typical atmospheric conditions, assuming both weather measurement theoretical values and values of direct measurements done at critical spans. Random errors were added to that set of measurements in order to estimate the conductor temperature in all ruling spans by means of the algorithm. These results were contrasted with values of temperature computed using the assumed theoretical measurements. The random errors were added

Algorithm 1 Proposed algorithm for DLR state estimation using WLS

1: **procedure** DLRSE($\mathbf{z}, OHL, \hat{\mathbf{x}}_0$) ▷ $\mathbf{z}$ is the measurement set
2: ▷ OHL has the line parameters
3: ▷ $\hat{\mathbf{x}}_0$ is the initial guess of the state vector
4:    $\hat{\mathbf{x}} \leftarrow \hat{\mathbf{x}}_0$
5:    $\epsilon \leftarrow 0.01$
6:    $e \leftarrow \infty$
7:    **while** $e \geq \epsilon$ **do**
8:        **if** $\exists \hat{\mathbf{x}}.T_S \leq -273$ **then**
9:            **return** error
10:            **break**
11:        **else**
12:            $\mathbf{h}(\mathbf{z}, \hat{\mathbf{x}}) \leftarrow \mathrm{h}(\mathbf{z}, \hat{\mathbf{x}}, OHL)$ ▷ Measurement functions
13:            $\mathbf{W} \leftarrow \mathrm{diag}\left(\begin{bmatrix} 1/\sigma_1{}^2 & 1/\sigma_2{}^2 & \ldots & 1/\sigma_i{}^2 \end{bmatrix}^T\right)$ ▷ Weights matrix
14:            $\mathbf{H} \leftarrow \partial \mathbf{h}(\mathbf{z}, \mathbf{x}) / \partial \mathbf{x}$ ▷ Jocabian matrix
15:            $\Delta\hat{\mathbf{x}} \leftarrow \left[[\mathbf{H}]^T [\mathbf{W}] [\mathbf{H}]\right]^{-1} [\mathbf{H}]^T [\mathbf{W}] [\mathbf{h}(\mathbf{z}, \hat{\mathbf{x}})]$
16:            $\hat{\mathbf{x}} \leftarrow \hat{\mathbf{x}} - \Delta\hat{\mathbf{x}}$
17:            $e \leftarrow \max |\Delta\hat{\mathbf{x}}|$
18:            **if** $\exists \mathrm{Im}(\Delta\hat{\mathbf{x}}) \neq 0$ **then**
19:                **return** error
20:                **break**
21:            **end if**
22:        **end if**
23:    **end while**
24:    **return** $\hat{\mathbf{x}}$
25: **end procedure**

Table 1: Direct and indirect measurements accuracy

	Name	Accuracy	Units	
NWP	T_a	2	[K]	[40]
	ϑ	35	[%]	[3, 40]
	δ	11.25	[°]	[3]
Down scaling	T_a	1	[K]	[11]
	ϑ	20	[%]	[11]
	δ	11.25	[°]	[3]
Direct measurements	T_S	0.5	[K]	[5]
	D	2.5	[cm]	[41]
	H	0.03	[%]	
	v, i	0.3	[%]	

assuming a normal probability distribution with mean 0 and a standard deviation (σ) assumed as one third of the measurement's accuracy. The accuracy for each kind of measurements is shown in Table 1.

The data used in the simulations corresponds to the OHL identified as BR-1 located in Iceland and operated by LandsNet. This OHL has 30 ruling spans as shown Figure 3, with a rate voltage of 220 [kV]. More information about OHL design and location is available in [20]. Close to the influence area of BR-1 there are identified 16 weather stations. Thus, to simulate the atmospheric conditions, the reports of those stations are used to interpolate the wind speed and direction and the ambient temperature through biharmonic splines (nowcasting). The atmospheric conditions were interpolated in the middle of each ruling span and assumed constant along that same span. A more complex model of weather nowcasting is out of the scope of this work because of the aim of this simulation is to evaluate the proposed SE algorithm under typical conditions. The interpolation were carried out at 18:00 18.04.2016 with atmospheric values got from Icelandic Met Office (as shown in Table 2). Finally, availability of two models of weather nowcasting were supposed: one to down scaling [11, 40] and other from a numerical weather prediction model (NWP), commonly found on the Web.

For direct measurements, a set of critical ruling spans was defined based on the weather variation for a typical day [20]. These critical ruling spans are $1, 10, 11, 12, 14, 15, 17$. However, the spans $10, 11, 12$ and $14, 15$ are close to each other, hence it is assumed that only four measurement devices are installed

Table 2: Weather station measurements at 18:00 18.04.2016

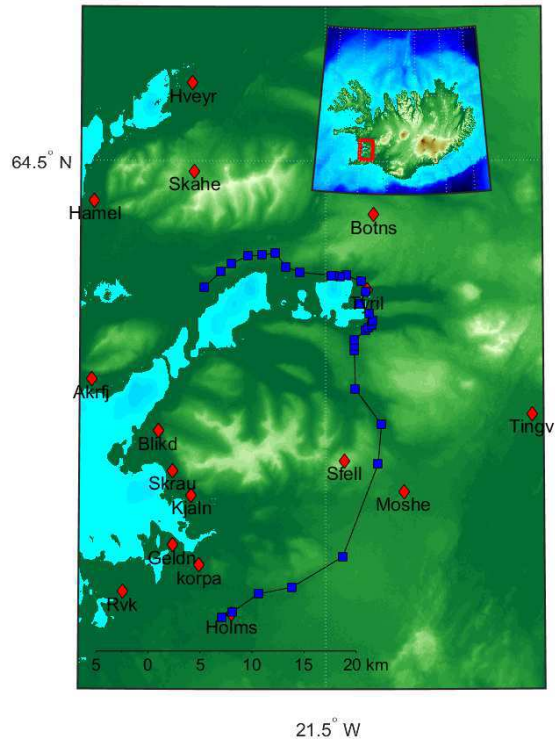| Name	T_a [°C]	ϑ [m/s]	Wind Direction [°]	Name	T_a [°C]	ϑ [m/s]	Wind Direction [°]
Rvk	3.0	3	225	Moshe	-0.5	4	-68
Holms	2.1	4	225	Tingv	2.5	3	270
Korpa	2.7	3	202	Akrfj	1.7	6	202
Geldn	3.1	3	202	Tyril	2.0	3	135
Kjaln	2.0	5	247	Botns	-3.5	5	270
Skrau	2.1	7	202	Skahe	-3.5	7	225
Blikd	1.8	5	247	Hamel	1.3	4	225
Sfell	-4.7	4	-68	Hveyr	1.5	5	225

Figure 3: Location of BR1-OHL ruling spans (blues squares) and nearby weather stations (red diamonds)

Table 3: Direct Measurements at 18:00 18.04.2016

	$z_{\text{Theor.}}$	$z_{measured}$ $z_{\text{Theor.}} + e$	Ruling Span	Span	Units
v_k	$-125.78 + j26.667$	$-125.60 + j26.63$	-	-	[kV]
i_k	$-518.32 + j486.70$	$-517.26 + j486.07$	-	-	[A]
v_m	$-111.32 + j37.853$	$-111.39 + j37.95$	-	-	[kV]
i_m	$513.00 - j506.26$	$511.86 - j505.74$	-	-	[A]
T_S	16.8	16.7	17	1	[°C]
H_1	25.356	25.353	1	1	[kN]
H_{15}	15.698	15.696	15	1	[kN]
D_{11}	10.38	10.39	11	1	[m]

Table 4: Indirect Measurements at 18:00 18.04.2016

Ruling Span	$z_{\text{Theor.}}$ T_a [°C]	ϑ [m/s]	δ [°]	$z_{down\,scaling}$ T_a [°C]	ϑ [m/s]	δ [°]	z_{NWP} T_a [°C]	ϑ [m/s]	δ [°]	Ruling Span	$z_{\text{Theor.}}$ T_a [°C]	ϑ [m/s]	δ [°]	$z_{down\,scaling}$ T_a [°C]	ϑ [m/s]	δ [°]	z_{NWP} T_a [°C]	ϑ [m/s]	δ [°]
1	2.3	3.8	32	2.6	3.8	32	1.8	4.4	32	16	2.1	2.8	16	2.0	2.8	25	1.3	3.2	13
2	1.2	4.4	46	1.3	4.9	40	2.1	3.6	44	17	2.0	3.0	15	2.3	3.1	21	2.4	2.7	16
3	-1.0	4.7	40	-0.7	4.8	39	-0.6	4.5	35	18	1.7	3.1	1	0.9	3.2	3	2.4	3.0	0
4	-3.5	4.6	66	-3.4	4.5	70	-4.7	5.5	65	19	0.8	3.5	48	1.4	3.5	49	0.7	4.1	50
5	-3.9	4.2	35	-4.0	4.5	36	-4.8	4.2	36	20	-0.1	3.8	52	-0.6	3.4	53	1.5	3.9	49
6	-1.4	3.6	31	-1.7	3.9	32	-0.9	4.2	27	21	-0.5	4.0	54	-0.3	4.1	51	-1.2	3.6	51
7	-1.0	3.3	82	-1.4	2.8	82	-1.8	3.6	79	22	-0.8	4.1	56	-1.0	4.0	49	-0.5	4.5	58
8	-0.2	3.1	10	0.2	3.2	9	-0.9	3.2	11	23	-1.9	4.7	64	-2.1	4.6	58	-1.2	5.7	66
9	0.6	3.0	41	0.5	3.0	40	1.0	3.0	45	24	-2.9	5.4	77	-3.4	5.9	76	-2.9	3.8	83
10	0.8	3.0	46	1.3	3.0	43	1.3	3.3	46	25	-3.3	5.8	57	-3.2	6.3	53	-3.6	5.4	55
11	1.4	2.9	9	1.4	2.7	17	2.1	2.5	2	26	-3.6	6.2	70	-3.2	5.9	69	-4.4	5.6	62
12	1.9	2.8	2	1.7	3.2	0	2.0	2.6	4	27	-3.9	6.5	62	-3.8	6.8	63	-3.5	6.6	65
13	2.1	2.8	9	2.6	2.7	11	3.6	2.7	12	28	-4.0	6.8	43	-3.9	6.8	38	-3.5	5.6	44
14	2.2	2.8	55	2.4	3.1	55	1.5	3.4	59	29	-4.0	7.0	29	-4.2	6.9	29	-3.5	6.6	32
15	2.2	2.8	37	2.4	3.0	39	1.8	2.9	43	30	-3.7	7.0	19	-3.7	7.6	21	-3.5	5.5	11

in spans $1, 11, 15, 17$. The initial guess values of $\hat{\mathbf{x}}_0$ for starting the SE algorithm are $R = 3.83$ [Ω], $X_L = 25.2$ [Ω], $Y_C = 164$ [μS] and $T_S = 40$ [°C]. These were taken from the OHL datasheet and T_S is the design maximum allowable temperature of the conductor.

4.1. Performance of the Algorithm in a generic application example

A generic example was chosen to evaluate the algorithm performance, adding random errors to the assumed theoretical values. The location and the values for both theoretical and simulated direct measurements are shown in Table 3. It is assumed that the PMUs are located at the ends of the OHL and the direct measurement devices are located at the ruling spans 1,11,15,17. These measurements are simulated adding random errors to the theoretical values as previously explained. The interpolated indirect measurements are shown in Table 4. Under these conditions, the estimated values of $\widehat{T}_S$ obtained with the algorithm and the theoretical values of T_S in each ruling span are shown in Figure 4, along with the errors between them. The algorithm converged in 4 iterations and the maximum error was $e \approx 2$[K] in the ruling span 16.

4.2. Impact of measurement error on SE accuracy

To assess the overall performance of the algorithm, 1000 cases were run adding normal random errors to the measurements. The procedure was executed on a standard laptop with 8 GB of RAM memory and a processor Intel® Core i5-1.70 GHz, obtaining an average time of 2.6 [s] with 3 or 4 iterations in each run. Figure 5 shows the temperature estimated through standard box plots, where the maximum distance between the upper and lower whiskers was ≈ 8 [K] located in the ruling span 13. Figure 6 shows the comparison between uncertainties obtained by using the estimation algorithm and computed with the two assumed weather models. The uncertainty was assumed as three times the standard deviation. The standard deviation in each ruling span was computed with the errors obtained in each one of the 1000 runs. As a result, in all ruling spans the uncertainty obtained in the computed temperature was lower (closer to the theoretical value) when the proposed algorithm was used (in comparison to using only weather reports). Additionally, the influence of direct measurements can be appreciated in the ruling spans 1,11,15 and 17.
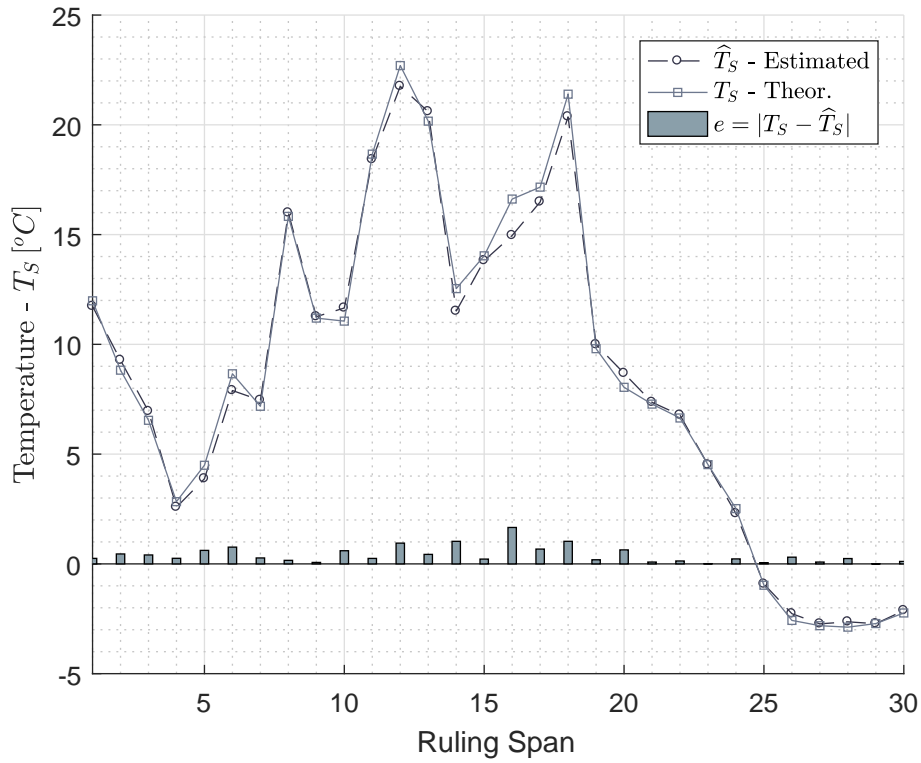
Figure 4: Estimated temperature by using the proposed algorithm, theoretical temperature values and error between both for each r
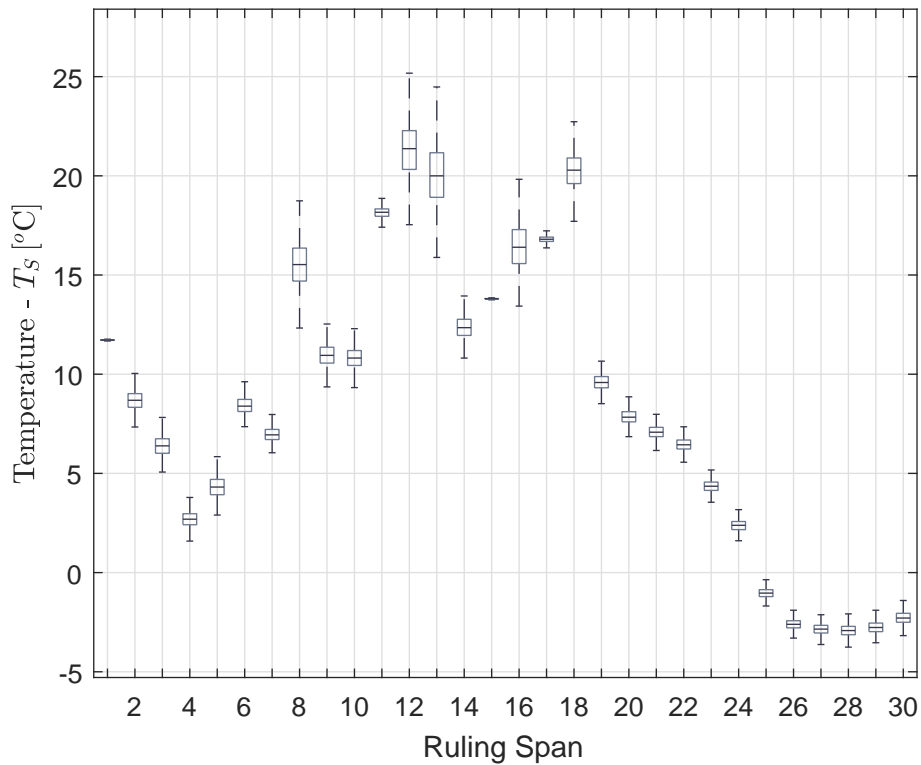

Figure 5: Box plots for estimated temperatures with proposed algorithm in each ruling span

4.3. Influence of direct measurements on close spans

The influence of direct measurements in the estimation of temperature in spans that are not directly monitored is analyzed through a comparison of three scenarios:
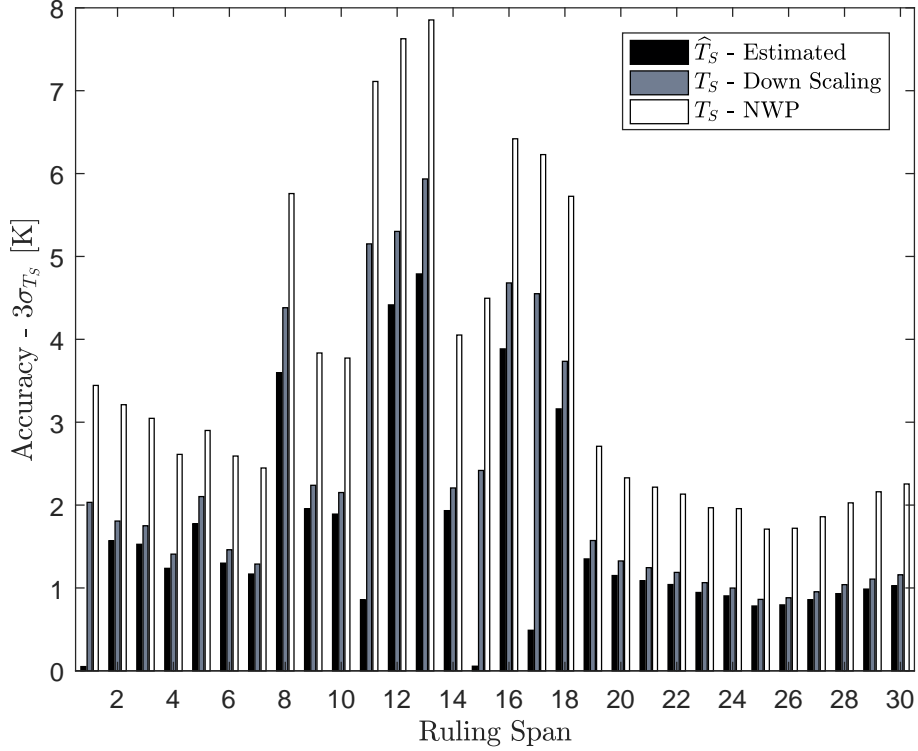
1. Using only PMU and nowcasting

11

Figure 6: Comparison of temperature estimated using the proposed algorithm, computed from NWP and from downscaling atmospheric models in each ruling span. Uncertainty was assumed as three times the standard deviation of error

2. Adding direct measurements to PMU and nowcasting
3. Adding a nowcasting update using direct measurements

A new interpolation is carried out for weather update, assuming the ambient temperature, solar radiation and wind direction of the previous weather nowcasting (in this work, the down scaling model) and including a new wind speed in the spans with direct measurements. This new wind speed is an average wind speed [42] computed according to [12] using the previous assumed atmospheric values. As a result, of considering a new weather nowcasting, which is based on results of a previous interpolation a higher weight is added to these measurements in the state estimation impacting the results. With the aim of avoiding this undesirable effect that changes results, the computing of the matrix of weights $\mathbf{W}$ is modified, multiplying by $\sqrt{2}$ the standard deviation in both the previous and the new nowcasting. Hence, the average wind speed update only influences the estimation of ruling spans located close to direct measurements. The cost of including the weather update is an increase in processing time (3.1 [s]) as a consequence of using a new nowcasting.

The uncertainty computed in the three scenarios with 1000 simulations is shown in Figure 7, where the influence of the direct measurements at local level (ruling spans 1,11,15 and 17) is observed. The influence of weather update over ruling spans 8,9,10,12,13,14,16 and 18, which are close to the location of direct measurements, can be observed, lowering uncertainty. The error increases in ruling spans 2 to 4 as a consequence of using biharmonic spline to update weather nowcasting. In these locations, it was observed that wind increased its value when the interpolation was carried out, thus that error can be associated to the weather nowcasting model instead of the state estimation algorithm. Authors believe that with a more accurate model of weather nowcasting update, the estimation of conductor temperature can be improved. This matter for future research and therefore, out of the scope of this work.

According to the previous simulation, the maximum errors obtained are ± 4.2 [K] and ± 2.9 [K] with confidence levels of 99.7% ($3\sigma_{T_S}$) and 95% respectively. Assuming the acceptable error margin given by the CIGRE [10] of ± 20 [cm] in sag estimation which is equivalent to 3.8 [K] in the ruling span 13 (where the maximum error was obtained) at a conductor temperature of 20 [°C]; this margin is achieved in all ruling spans, provided a confidence level of 95%. If higher reliability is required, a direct measurement device must be installed on ruling span 13 or a more accurate nowcasting model must be used.
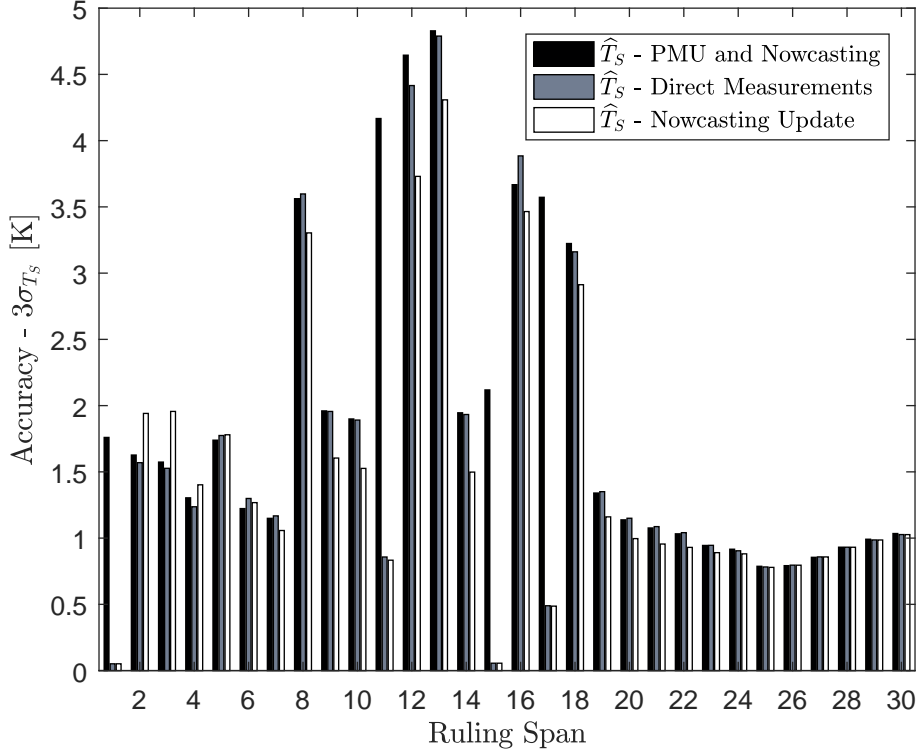
Figure 7: Comparison of accuracy between temperature estimated using PMU and weather nowcasting, direct measurements in ruling spans (1,11,15,17), and a weather nowcasting carried out means of updating from direct measurements

5. Discussion and Conclusion

This paper proposes the integration of direct and indirect DLR measurements by means of incorporating the equivalent resistance and the total losses into a new algorithm to estimate temperature of all OHLs ruling spans, thus minimizing measurement errors. The presented algorithm takes advantage of the developments in weather nowcasting as well as benefitting from the high accuracy of devices used for direct measurement.

The SE algorithm can be used with the aim of both reducing congestion and increasing reliability in OHLs. This algorithm runs if at least PMU measurements and a weather nowcasting are available. Furthermore, the algorithm has the ability of including direct measurements in critical spans in order to improve estimation's accuracy. These measurements (tension, sag and temperature) have a high impact in the temperature estimation's accuracy in the spans where devices are located. Additionally, redundant measurements can be included to increase reliability and security of the DLR systems. Nevertheless, if the algorithm is operated only with PMU measurements and weather nowcasting exist the risk of increasing the error in the estimation.

In this work, the expressions to implement the SE algorithm were derived, for example, a state equation to compute the temperature in the conductor using tension and sag measurements, the derivatives of CIGRE standard to compute temperature from atmospheric conditions, the approximation of cosh to the first two terms of the Taylor series expansion and approximations in the computing of uncertainty propagation. All these expressions can be changed in the proposed algorithm, according to research needs. As an example, linear, simplified or complex models such as plastic elongation can be used, as well as heat transfer equilibrium approximations, among others. To carry out these changes it is necessary to formulate the measurement functions, the Jacobian and the weight matrix.

Finally, the algorithm was tested in a real OHL configuration and simulating typical atmospheric conditions. Simulations show that it is fast and computationally efficient, with computing times less than three seconds. This is a short time considering that a set of nonlinear equations must be solved and a complete overview of the conductor temperature along the OHL is provided, with errors less than ± 4 [K].

AppendixA. Measurement Functions - h(z, x̂)

The vector (19) related the DLR measurements with the state vector as follows:

1. $\mathrm{Re}\,(h_v\,(\mathbf{z}, \mathbf{x}))$ (A.1), $\mathrm{Im}\,(h_v\,(\mathbf{z}, \mathbf{x}))$ (A.2), $\mathrm{Re}\,(h_i\,(\mathbf{z}, \mathbf{x}))$ (A.3), $\mathrm{Im}\,(h_i\,(\mathbf{z}, \mathbf{x}))$ (A.4) are the measurement functions that related the state variables RLC with PMU measurements. These relationships are obtained from (7) and (8).

$$\mathrm{Re}\,(h_v\,(\mathbf{x}, \mathbf{z})) = \mathrm{Re}\,(v_k) - \left(-\frac{\mathrm{Re}\,(v_m)\,X_L Y_C}{2}\mathrm{Re}\,(v_m) - \frac{\mathrm{Im}\,(v_m)\,Y_C R}{2} + \mathrm{Im}\,(i_m)\,X_L - \mathrm{Re}\,(i_m)\,R \right) \quad \text{(A.1)}$$

$$\mathrm{Im}\,(h_v\,(\mathbf{x}, \mathbf{z})) = \mathrm{Im}\,(v_k) - \left(-\frac{\mathrm{Im}\,(v_m)\,X_L Y_C}{2} + \mathrm{Im}\,(v_m) + \frac{\mathrm{Re}\,(v_m)\,Y_C R}{2} - \mathrm{Im}\,(i_m)\,R - \mathrm{Re}\,(i_m)\,X_L \right) \quad \text{(A.2)}$$

$$\mathrm{Re}\,(h_i\,(\mathbf{x}, \mathbf{z})) = \mathrm{Re}\,(i_k) - \left(\frac{\mathrm{Im}\,(v_m)\,X_L Y_C{}^2}{4} - \mathrm{Im}\,(v_m)\,Y_C - \right.$$
$$\left. \frac{\mathrm{Re}\,(v_m)\,Y_C{}^2 R}{4} + \frac{\mathrm{Re}\,(i_m)\,X_L Y_C}{2} - \mathrm{Re}\,(i_m) + \frac{\mathrm{Im}\,(i_m)\,Y_C R}{2} \right) \quad \text{(A.3)}$$

$$\mathrm{Im}\,(h_i\,(\mathbf{x}, \mathbf{z})) = \mathrm{Im}\,(i_k) - \left(-\frac{\mathrm{Re}\,(v_m)\,X_L Y_C{}^2}{4} + \mathrm{Re}\,(v_m)\,Y_C - \right.$$
$$\left. \frac{\mathrm{Im}\,(v_m)\,Y_C{}^2 R}{4} + \frac{\mathrm{Im}\,(i_m)\,X_L Y_C}{2} - \mathrm{Im}\,(i_m) - \frac{\mathrm{Re}\,(i_m)\,Y_C R}{2} \right) \quad \text{(A.4)}$$

2. $h_R\,(\mathbf{z}, \mathbf{x})$ (A.5) and $h_P\,(\mathbf{z}, \mathbf{x})$ (A.6) are the equations of integration which relate the temperature in each ruling span with the equivalent OHL resistance (13) and the losses on the entire conductor (12).

$$h_R\,(\mathbf{z}, \mathbf{x}) = R - \sum_{n=1}^{N} R_n\,(T_{S_n}) \quad \text{(A.5)}$$

$$h_P\,(\mathbf{z}, \mathbf{x}) = \left| i_k - \frac{v_k Y}{2} \right|^2 R - \left| \frac{v_m Y}{2} - i_m \right|^2 \sum_{n=1}^{N} R_n\,(T_{S_n}) \quad \text{(A.6)}$$

3. $\mathbf{h}_Q\,(\mathbf{z}, \mathbf{x})$ (A.7) is the set of measurement functions used to model the heat transfer equilibrium on each ruling span, related the atmospheric conditions and the current intensity with the temperature of the conductor.

$$h_Q\,(\mathbf{z}, \mathbf{x}) = Q_C + Q_R - (Q_J + Q_S) \quad \text{(A.7)}$$

4. $\mathbf{h}_T\,(\mathbf{z}, \mathbf{x})$ (A.8) is the residual between temperature measurements on the conductor and the state variables of temperature.

$$h_T\,(\mathbf{z}, \mathbf{x}) = \mathbf{z}\,[T_S] - \mathbf{x}\,[T_S] \quad \text{(A.8)}$$

5. $\mathbf{h}_H\,(\mathbf{z}, \mathbf{x})$ (A.9) relates the mechanical tension measurements with state variables of temperature by means of using the state change equation (2).

$$h_H\,(\mathbf{z}, \mathbf{x}) = \mathbf{z}\,[H] - H\,(\mathbf{x}\,[T_S]) \quad \text{(A.9)}$$

6. $\mathbf{h}_D\,(\mathbf{z}, \mathbf{x})$ (A.10) relates the sag measurements with temperature through the centenary series expansion (5) and state change equation (2).

$$h_D\,(\mathbf{z}, \mathbf{x}) = H\,(\mathbf{z}\,[D]) - H\,(\mathbf{x}\,[T_S]) \quad \text{(A.10)}$$

AppendixB. Least Square Weights - Matrix [W]

The following assumptions are made in this work for selecting the weights in the Least Square estimation:

1. Direct σ.
   Standard deviations for voltages σ_v, currents σ_i, and direct measurements of temperature $\boldsymbol{\sigma}_{T_S}$ and tension $\boldsymbol{\sigma}_H$ are assumed as a third part of the measurement accuracy.

2. Indirect σ

   Given that Due to the remaining measurement functions are calculated using indirect measurements, the uncertainty is propagated. Therefore, the uncertainty is computed by means of (B.1).

$$\sigma_{h(\mathbf{z},\mathbf{x})} = \sqrt{\left(\frac{\partial h(\mathbf{z},\mathbf{x})}{\partial z_1}\sigma_{z_1}\right)^2 + \left(\frac{\partial h(\mathbf{z},\mathbf{x})}{\partial z_2}\sigma_{z_2}\right)^2 + \cdots + \left(\frac{\partial h(\mathbf{z},\mathbf{x})}{\partial z_N}\sigma_{z_N}\right)^2} \tag{B.1}$$

For function $h_R(\mathbf{z},\mathbf{x})$, it is considered that the resistance is indirectly measured by PMU. This can be approximated by means of (B.2), assuming that the shunt capacitance is negligible. As result, the standard deviation is computed with (B.3).

$$R \approx \mathrm{Re}\left(\frac{v_k - v_m}{i_{km}}\right) \tag{B.2}$$

$$\begin{aligned} \sigma_R &= \sqrt{\left(\frac{\partial R}{\partial v_k}\sigma_v\right)^2 + \left(\frac{\partial R}{\partial v_m}\sigma_v\right)^2 + \left(\frac{\partial R}{\partial i_{km}}\sigma_{i_{km}}\right)^2} \\ \frac{\partial R}{\partial v_k} &= \frac{\cos(\angle v_k - \angle i_{km})}{|i_{km}|} \\ \frac{\partial R}{\partial v_m} &= -\frac{\cos(\angle v_m - \angle i_{km})}{|i_{km}|} \\ \frac{\partial R}{\partial i_{km}} &= \frac{|v_k|\cos(\angle v_k - \angle i_{km}) - |v_m|\cos(\angle v_m - \angle i_{km})}{|i_{km}|^2} \end{aligned} \tag{B.3}$$

For function $h_P(\mathbf{z},\mathbf{x})$ it is assumed that the losses i^2R are indirectly measured. Consequently, the standard deviation is calculated with (B.4), where R and σ_R are taken from (B.2) and (B.3).

$$\sigma_{h_P(\mathbf{z},\mathbf{x})} = \sqrt{(2|i|R\sigma_i)^2 + \left(|i|^2\sigma_R\right)^2} \tag{B.4}$$

For sag measurements, $\mathbf{h}_D(\mathbf{z},\mathbf{x})$ represents the tension in function of sag, thus, the uncertainty is computed with (B.5), provided that the parabolic approximation in (4) is used.

$$\sigma_{h_D(\mathbf{z},\mathbf{x})} = \frac{s^2 m_c g}{8D^2}\sigma_D \tag{B.5}$$

The standard deviation for heat transfer equilibrium is computed with (B.6), where the derivatives are approximated using the expressions given in [32]. For wind speed below of 0.5 [m/s] $\partial Q_C/\partial T_a = 0$, and $\partial Q_C/\partial \delta = 0$. Due to stability problems presented in the estimation for values of σ_δ greater than 6 [°], in this work, $\partial Q_C/\partial \delta$ was assumed as 0. This problem will be addressed to future research.

$$\begin{aligned} \sigma_{h_Q(\mathbf{z},\mathbf{x})} &= \sqrt{\left(\frac{\partial Q_R}{\partial T_a}\sigma_{T_a} + \frac{\partial Q_C}{\partial T_a}\sigma_{T_a}\right)^2 + \left(\frac{\partial Q_C}{\partial \vartheta}\sigma_\vartheta\right)^2 + \left(\frac{\partial Q_C}{\partial \delta}\sigma_\delta\right)^2 + \left(\frac{\partial Q_J}{\partial i_{km}}\sigma_{i_{km}}\right)^2 + \sigma_S^2} \\ \frac{\partial Q_J}{\partial i_{km}} &= 2i_{km}R'_{ref}(1 + \alpha(T_S - T_{ref})) \\ \frac{\partial Q_R}{\partial T_a} &= -4\pi d\epsilon\sigma_b(T_a + 273)^3 \\ \frac{\partial Q_C}{\partial T_a} &\approx -2.42\times10^{-2}\pi B_1\left(7.58\times10^4\rho_r\vartheta d\right)^n(A_2 + B_2\sin\delta^{m_1}) \\ \frac{\partial Q_C}{\partial \vartheta} &\approx \frac{2.42\times10^{-2}n\pi(T_S - T_a)B_1}{\vartheta}\left(7.58\times10^4\rho_r\vartheta d\right)^n(A_2 + B_2\sin\delta^{m_1}) \\ \frac{\partial Q_C}{\partial \delta} &\approx \frac{2.42\times10^{-2}\pi(T_S - T_a)B_1}{\sin\delta}\left(7.58\times10^4\rho_r\vartheta d\right)^n(B_2\sin\delta^{m_1}m_1\cos\delta) \end{aligned} \tag{B.6}$$

Finally, the weight matrix **W** has the form of (B.7).

$$[\mathbf{W}] = \mathrm{diag}\left[1/\sigma_v{}^2 \quad 1/\sigma_v{}^2 \quad 1/\sigma_i{}^2 \quad 1/\sigma_i{}^2 \quad 1/\sigma_{h_R}{}^2 \ldots \right.$$
$$\left. 1/\sigma_{h_P}{}^2 \quad 1/\boldsymbol{\sigma}_{h_Q}{}^2 \quad 1/\boldsymbol{\sigma}_{T_S}{}^2 \quad 1/\boldsymbol{\sigma}_H{}^2 \quad 1/\boldsymbol{\sigma}_{h_D}{}^2\right]^T \tag{B.7}$$

AppendixC. Partial Derivatives of the Measurement Functions - Jacobian Matrix [H]

Due to the complexity of deriving dH/dT_S from (2) in an analytical way, the derivative of inverse function (C.1) is used in this work for computing dH/dT_S, where $T_S = f(H)$ (C.2).

$$\left(f^{-1}\right)'(f(H)) = \frac{1}{f'(H)} \tag{C.1}$$

$$T_S = \frac{(R_s m_c g)^2}{\varepsilon_t 24}\left(\frac{1}{H^2} - \frac{1}{H_{T_{ref}}{}^2}\right) - \frac{H - H_{T_{ref}}}{EA\varepsilon_t} + T_{ref} \tag{C.2}$$

The derivative dT_S/dH is shown in (C.3).

$$\frac{dT_S}{dH} = -\frac{(R_s m_c g)^2}{12\varepsilon_t H^3} - \frac{1}{EA\varepsilon_t} \tag{C.3}$$

Partial derivatives for heat transfer equilibrium (C.4) to (C.7) were calculated using expressions presented in [32], where d is the diameter of the conductor, ε_m is the solar emissivity of the conductor surface (in this work assumed as 0.5), σ_B is the Stefan-Boltzmann constant, α is the temperature coefficient of resistance, $R'_{T_{ref}}$ is the resistivity per unit length at temperature T_{ref}, and $B1$, A_2 n, and m_2 are constants described in [32].

$$\frac{\partial Q_J}{\partial T_S} = |i|^2\, R'_{T_{ref}}\alpha \tag{C.4}$$

$$\frac{\partial Q_S}{\partial T_S} = 0 \tag{C.5}$$

$$\frac{\partial Q_R}{\partial T_S} = 4\pi d\varepsilon_m\sigma_B\left(T_S + 273\right)^3 \tag{C.6}$$

The partial derivative for natural cooling is shown in (C.7).

$$\frac{\partial Q_C}{\partial T_S} = 6.41 \times 10^{-16}\pi A_2 K_1{}^{m_2}\left(\frac{K_2 T_S{}^4 + K_3 T_S{}^3 + K_4 T_S{}^2 + K_5 T_S + K_6 + K_7}{K_8}\right)$$

$$K_1 = \frac{2gD^3\left(T_a - T_S\right)\left(-0.75 + 1.25 \times 10^{-4}\left(T_S + T_a\right)\right)}{\left(T_S + T_a + 546\right)\left(1.32 \times 10^{-5} + 4.75 \times 10^{-8}\left(T_S + T_a\right)\right)^2}$$

$$K_2 = \frac{2 - m_2}{3}$$

$$K_3 = 2T_a + 3.87 \times 10^3 m_2 - 3.23 \times 10^3$$

$$K_4 = 2\left(1 + m_2\right)T_a{}^2 + \left(8.66 \times 10^2 m_2 - 6.23 \times 10^3\right)T_a + 3.94 \times 10^6 m_2 - 4.35 \times 10^6$$

$$K_5 = \frac{2 + 8m_2}{3}T_a{}^3 - \left(9.87 \times 10^3 m_2 + 2.78 \times 10^3\right)T_a{}^2 - 5.51 \times 10^6\left(1 + m_2\right)T_a + 4.99 \times 10^8 m_2 - 1.68 \times 10^9$$

$$K_6 = m_2 T_a{}^4 + \left(2.24 \times 10^2 - 6.87 \times 10^3 m_2\right)T_a{}^3 - \left(9.46 \times 10^6 m_2 + 1.16 \times 10^6\right)T_a{}^2$$

$$K_7 = -\left(1.07 \times 10^9 + 3.25 \times 10^9 m_2\right)T_a - 2.04 \times 10^{11}\left(1 + m_2\right)$$

$$K_8 = \left(T_S + T_a + 546\right)\left(1.32 \times 10^{-5} + 4.75 \times 10^{-8}\left(T_S + T_a\right)\right)\left(1.25 \times 10^{-4}\left(T_S + T_a\right) - 0.75\right) \tag{C.7}$$

During forced cooling, the partial derivative (C.8) is used, where the parameter k, depends on wind attack

angle (δ) and wind speed (ϑ) [32].

$$\frac{\partial Q_C}{\partial T_S} = k\pi B_1 \left(\frac{\rho_r \vartheta d}{4.75 \times 10^{-8} \left(T_a + T_S \right) + 1.32 \times 10^{-5}} \right)^n \left(7.2 \times 10^{-5} T_S + \right.$$
$$\left. 0.0242 - \frac{4.75 \times 10^{-8} n \left(3.6 \times 10^{-5} \left(T_a + T_S \right) + 0.0242 \right) \left(T_S - T_a \right)}{4.75 \times 10^{-8} \left(T_S + T_a \right) + 1.32 \times 10^{-5}} \right) \tag{C.8}$$

Finally, the elements of the Jacobian Matrix (23) are computed by means of (C.9) to (C.30).

Acknowledgment

References

[1] W. Winter, K. Elkington, G. Bareux, J. Kostevc, Pushing the Limits: Europe's New Grid: Innovative Tools to Combat Transmission Bottlenecks and Reduced Inertia, Power and Energy Magazine, IEEE 13 (1) (2015) 60–74. doi:10.1109/MPE.2014.2363534.

[2] S. D. Kim, M. M. Morcos, An Application of Dynamic Thermal Line Rating Control System to Up-Rate the Ampacity of Overhead Transmission Lines, Power Delivery, IEEE Transactions on 28 (2) (2013) 1231–1232. doi:10.1109/TPWRD.2012.2234940.

[3] D. Douglass, W. Chisholm, G. Davidson, I. Grant, K. Lindsey, M. Lancaster, D. Lawry, T. McCarthy, C. Nascimento, M. Pasha, J. Reding, T. Seppa, J. Toth, P. Waltz, Real-Time Overhead Transmission-Line Monitoring for Dynamic Rating, IEEE Transactions on Power Delivery 31 (3) (2016) 921–927. doi:10.1109/TPWRD.2014.2383915.

[4] M. A. Bucher, G. Andersson, Robust Corrective Control Measures in Power Systems With Dynamic Line Rating, IEEE Transactions on Power Systems 31 (3) (2016) 2034–2043. doi:10.1109/TPWRS.2015.2449753.

[5] E. Fernandez, I. Albizu, M. Bedialauneta, A. Mazon, P. Leite, Review of dynamic line rating systems for wind power integration, Renewable and Sustainable Energy Reviews 53 (2016) 80–92. doi:10.1016/j.rser.2015.07.149.

[6] D. L. Alvarez, J. A. Rosero, F. F. da Silva, C. L. Bak, E. E. Mombello, Dynamic line rating - technologies and challenges of pmu on overhead lines: A survey, in: 51st International Universities Power Engineering Conference (UPEC), IEEE Press, Coimbra, 2016, pp. 1–6. doi:10.1109/UPEC.2016.8114069. URL http://ieeexplore.ieee.org/document/8114069/

[7] H. Banakar, N. Alguacil, F. Galiana, Electrothermal Coordination Part I: Theory and Implementation Schemes, IEEE Transactions on Power Systems 20 (2) (2005) 798–805. doi:10.1109/TPWRS.2005.846196.

[8] B. Banerjee, D. Jayaweera, S. M. Islam, Optimal scheduling with dynamic line ratings and intermittent wind power, in: PES General Meeting — Conference Exposition, 2014 IEEE, 2014, pp. 1–5. doi:10.1109/PESGM.2014.6939381.

[9] M. Nick, O. Alizadeh-Mousavi, R. Cherkaoui, M. Paolone, Security Constrained Unit Commitment with Dynamic Thermal Line Rating, IEEE Transactions on Power Systems 31 (3) (2016) 2014–2025. doi:10.1109/TPWRS.2015.2445826.

[10] S. Rob, L. Jean-Louis, S. Tap, D. Dale, L. Mark, B. Gerhard, P. R. Watt George, F. Patrick, S. Michael, Guide for Application of Direct Real-time Monitoring Systems, CIGRE, Paris, 2012. URL http://www.e-cigre.org/

[11] D. M. Greenwood, J. P. Gentle, K. S. Myers, P. J. Davison, I. J. West, J. W. Bush, G. L. Ingram, M. C. M. Troffaes, A Comparison of Real-Time Thermal Rating Systems in the U.S. and the U.K., Power Delivery, IEEE Transactions on 29 (4) (2014) 1849–1858. doi:10.1109/TPWRD.2014.2299068.

[12] I. Albizu, E. Fernandez, P. Eguia, E. Torres, A. J. Mazon, Tension and Ampacity Monitoring System for Overhead Lines, Power Delivery, IEEE Transactions on 28 (1) (2013) 3–10. doi:10.1109/TPWRD.2012.2213308.

[13] C. R. Black, W. A. Chisholm, Key Considerations for the Selection of Dynamic Thermal Line Rating Systems, IEEE Transactions on Power Delivery 30 (5) (2015) 2154–2162. doi:10.1109/TPWRD.2014.2376275.

[14] S. Frank, J. Sexauer, S. Mohagheghi, Temperature-Dependent Power Flow, IEEE Transactions on Power Systems 28 (4) (2013) 4007–4018. doi:10.1109/TPWRS.2013.2266409.

[15] G. Sivanagaraju, S. Chakrabarti, S. C. Srivastava, Uncertainty in Transmission Line Parameters: Estimation and Impact on Line Current Differential Protection, Instrumentation and Measurement, IEEE Transactions on PP (99) (2013) 1. doi:10.1109/TIM.2013.2292276.

[16] V. Cecchi, A. S. Leger, K. Miu, C. O. Nwankpa, Incorporating Temperature Variations Into Transmission-Line Models, IEEE Transactions on Power Delivery 26 (4) (2011) 2189–2196. doi:10.1109/TPWRD.2011.2159520.

[17] Y. Du, Y. Liao, On-line estimation of transmission line parameters, temperature and sag using PMU measurements, Electric Power Systems Research 93 (2012) 39–45. doi:10.1016/j.epsr.2012.07.007.

PMU $\dfrac{d\,\mathrm{Re}\,(h_v\,(\mathbf{z},\mathbf{x}))}{d\mathbf{x}}$	$\dfrac{\partial\,\mathrm{Re}\,(h_v)}{\partial R}=\dfrac{\mathrm{Im}\,(v_m)\,Y_C}{2}+\mathrm{Re}\,(i_m)$	(C.9)
	$\dfrac{\partial\,\mathrm{Re}\,(h_v)}{\partial X_L}=\dfrac{\mathrm{Re}\,(v_m)\,Y_C}{2}-\mathrm{Im}\,(i_m)$	(C.10)
	$\dfrac{\partial\,\mathrm{Re}\,(h_v)}{\partial Y_C}=\dfrac{\mathrm{Re}\,(v_m)\,X_L+\mathrm{Im}\,(v_m)\,R}{2}$	(C.11)
PMU $\dfrac{d\,\mathrm{Im}\,(h_v\,(\mathbf{z},\mathbf{x}))}{d\mathbf{x}}$	$\dfrac{\partial\,\mathrm{Im}\,(h_v)}{\partial R}=-\dfrac{\mathrm{Re}\,(v_m)\,Y_C}{2}+\mathrm{Im}\,(i_m)$	(C.12)
	$\dfrac{\partial\,\mathrm{Im}\,(h_v)}{\partial X_L}=\dfrac{\mathrm{Im}\,(v_m)\,Y_C}{2}+\mathrm{Re}\,(i_m)$	(C.13)
	$\dfrac{\partial\,\mathrm{Im}\,(h_v)}{\partial Y_C}=\dfrac{\mathrm{Im}\,(v_m)\,X_L-\mathrm{Re}\,(v_m)\,R}{2}$	(C.14)
PMU $\dfrac{d\,\mathrm{Re}\,(h_i\,(\mathbf{z},\mathbf{x}))}{d\mathbf{x}}$	$\dfrac{\partial\,\mathrm{Re}\,(h_i)}{\partial R}=-\dfrac{\mathrm{Im}\,(i_m)\,Y_C}{2}+\dfrac{\mathrm{Re}\,(v_m)\,Y_C{}^2}{4}$	(C.15)
	$\dfrac{\partial\,\mathrm{Re}\,(h_i)}{\partial X_L}=-\dfrac{\mathrm{Re}\,(i_m)\,Y_C}{2}-\dfrac{\mathrm{Im}\,(v_m)\,Y_C{}^2}{4}$	(C.16)
	$\dfrac{\partial\,\mathrm{Re}\,(h_i)}{\partial Y_C}=\mathrm{Im}\,(v_m)+\dfrac{-\mathrm{Im}\,(v_m)\,Y_C X_L+\mathrm{Re}\,(v_m)\,Y_C R-\mathrm{Re}\,(i_m)\,X_L-\mathrm{Im}\,(i_m)\,R}{2}$	(C.17)
PMU $\dfrac{d\,\mathrm{Im}\,(h_i\,(\mathbf{z},\mathbf{x}))}{d\mathbf{x}}$	$\dfrac{\partial\,\mathrm{Im}\,(h_i)}{\partial R}=\dfrac{\mathrm{Re}\,(i_m)\,Y_C}{2}+\dfrac{\mathrm{Im}\,(v_m)\,Y_C{}^2}{4}$	(C.18)
	$\dfrac{\partial\,\mathrm{Im}\,(h_i)}{\partial X_L}=-\dfrac{\mathrm{Im}\,(i_m)\,Y_C}{2}+\dfrac{\mathrm{Re}\,(v_m)\,Y_C{}^2}{4}$	(C.19)
	$\dfrac{\partial\,\mathrm{Im}\,(h_i)}{\partial Y_C}=-\mathrm{Re}\,(v_m)+\dfrac{\mathrm{Re}\,(v_m)\,Y_C X_L+\mathrm{Im}\,(v_m)\,Y_C R-\mathrm{Im}\,(i_m)\,X_L+\mathrm{Re}\,(i_m)\,R}{2}$	(C.20)
Resistance $\dfrac{dh_R\,(\mathbf{z},\mathbf{x})}{d\mathbf{x}}$	$\dfrac{\partial h_R}{\partial R}=1$	(C.21)
	$\dfrac{\partial h_R}{\partial T_S}=-R'_{T_{ref}}\ell\alpha$	(C.22)
Losses $\dfrac{dh_P\,(\mathbf{z},\mathbf{x})}{d\mathbf{x}}$	$\dfrac{\partial h_P}{\partial R}=\left|i_k-\dfrac{v_k Y}{2}\right|^2$	(C.23)
	$\dfrac{\partial h_P}{\partial Y_C}=\left[\left(\mathrm{Re}\,(i_k)+\dfrac{\mathrm{Im}\,(v_k)\,Y_C}{2}\right)\mathrm{Im}\,(v_k)-\left(\mathrm{Im}\,(i_k)-\dfrac{\mathrm{Re}\,(v_k)\,Y_C}{2}\right)\mathrm{Re}\,(v_k)\right]\cdot R-$ $\left[\left(\mathrm{Re}\,(i_m)+\dfrac{\mathrm{Im}\,(v_m)\,Y_C}{2}\right)\mathrm{Im}\,(v_m)+\left(\dfrac{\mathrm{Re}\,(v_m)\,Y_C}{2}-\mathrm{Im}\,(i_m)\right)\mathrm{Re}\,(v_m)\right]\cdot$ $\displaystyle\sum_{n=1}^{N}R'_{T_{ref}}\ell\left(1+\alpha\left(T_S-T_{ref}\right)\right)$	(C.24)
	$\dfrac{\partial h_P}{\partial T_S}=-\left|\dfrac{v_m Y}{2}-i_m\right|^2 R'_{T_{ref}}\ell\alpha$	(C.25)
Heat transfer $\dfrac{dh_Q\,(\mathbf{z},\mathbf{x})}{d\mathbf{x}}$	$\dfrac{\partial h_Q}{\partial Y_C}=-\left(\left(\mathrm{Re}\,(i_m)+\dfrac{\mathrm{Im}\,(v_m)\,Y_C}{2}\right)\mathrm{Im}\,(v_m)-\left(\mathrm{Im}\,(i_m)-\dfrac{\mathrm{Re}\,(v_m)\,Y_C}{2}\right)\mathrm{Re}\,(v_m)\right)\cdot$ $R'_{T_{ref}}\left(1+\alpha\left(T_S-T_{ref}\right)\right)$	(C.26)
	$\dfrac{\partial h_Q}{\partial T_S}=\dfrac{\partial Q_C}{\partial T_S}+\dfrac{\partial Q_R}{\partial T_S}-\left(\dfrac{\partial Q_J}{\partial T_S}+\dfrac{\partial Q_S}{\partial T_S}\right)$	(C.27)
Temperature $\dfrac{dh_{T_S}\,(\mathbf{z},\mathbf{x})}{d\mathbf{x}}$	$\dfrac{\partial h_T}{\partial T_S}=-1$	(C.28)
Tension $\dfrac{dh_H\,(\mathbf{z},\mathbf{x})}{d\mathbf{x}}$	$\dfrac{\partial h_H}{\partial T_S}=-\dfrac{1}{\dfrac{(R_s m_c g)^2}{12\varepsilon_t H^3}+\dfrac{1}{EA\varepsilon_t}}$	(C.29)
Sag $\dfrac{dh_D\,(\mathbf{z},\mathbf{x})}{d\mathbf{x}}$	$\dfrac{\partial h_D}{\partial T_S}=-\dfrac{1}{\dfrac{(R_s m_c g)^2}{12\varepsilon_t H\,(D)^3}+\dfrac{1}{EA\varepsilon_t}}$	(C.30)

[18] R. Mai, L. Fu, X. HaiBo, Dynamic Line Rating estimator with synchronized phasor measurement, in: 2011 International Conference on Advanced Power System Automation and Protection, Vol. 2, IEEE, 2011, pp. 940–945. doi:10.1109/APAP.2011.6180545.
URL http://ieeexplore.ieee.org/document/6180545/

[19] C. Rehtanz, Synchrophasor based thermal overhead line monitoring considering line spans and thermal transients, IET Generation, Transmission & Distribution 10 (5) (2016) 1232–1239(7). doi:10.1049/iet-gtd.2015.0852.

[20] D. Alvarez, F. M. F. da Silva, C. L. Bak, E. Mombello, J. Rosero, D. Olason, A Methodology to Assess PMU in the Estimation of Dynamic Line Rating, Generation, Transmission Distribution, IET- Under Review - Round 1.

[21] E. M. Carlini, C. Pisani, A. Vaccaro, D. Villacci, Dynamic Line Rating monitoring in WAMS: Challenges and practical solutions, in: 2015 IEEE 1st International Forum on Research and Technologies for Society and Industry, RTSI 2015 - Proceedings, IEEE, 2015, pp. 359–364. doi:10.1109/RTSI.2015.7325124.

[22] M. Weibel, W. Sattinger, P. Rothermann, U. Steinegger, M. Zima, G. Biedenbach, Overhead line temperature monitoring pilot project, in: CIGRE 2006 Session, CIGRE_B2-311, 2006.
URL https://e-cigre.org/publication/B2-311{_}2006-overhead-line-temperature-monitoring-pilot-project

[23] I. Cotton, J. Teh, Critical span identification model for dynamic thermal rating system placement, IET Generation, Transmission & Distribution 9 (16) (2015) 2644–2652. doi:10.1049/iet-gtd.2015.0601.

[24] M. Matus, D. Saez, M. Favley, C. Suazo-Martinez, J. Moya, G. Jimenez-Estevez, R. Palma-Behnke, G. Olguin, P. Jorquera, Identification of Critical Spans for Monitoring Systems in Dynamic Thermal Rating, Power Delivery, IEEE Transactions on 27 (2) (2012) 1002–1009. doi:10.1109/TPWRD.2012.2185254.

[25] J. L. Aznarte, N. Siebert, Dynamic Line Rating Using Numerical Weather Predictions and Machine Learning: A Case Study, IEEE Transactions on Power Delivery 32 (1) (2017) 335–343. doi:10.1109/TPWRD.2016.2543818.

[26] D. J. Morrow, J. Fu, S. M. Abdelkader, Experimentally validated partial least squares model for dynamic line rating, Renewable Power Generation, IET 8 (3) (2014) 260–268. doi:10.1049/iet-rpg.2013.0097.

[27] I. Albizu, E. Fernaandez, A. J. Mazoon, J. Bengoechea, Influence of the conductor temperature error on the overhead line ampacity monitoring systems, Generation, Transmission Distribution, IET 5 (4) (2011) 440–447. doi:10.1049/iet-gtd.2010.0470.

[28] A. Michiorri, P. C. Taylor, S. C. E. Jupe, Overhead line real-time rating estimation algorithm : description and validation, Proc. IMechE - J. Power and Energy 224 (A) (2009) 293–304. doi:10.1243/09576509JPE859.

[29] E. M. Carlini, C. Pisani, A. Vaccaro, D. Villacci, A reliable computing framework for dynamic line rating of overhead lines, Electric Power Systems Research 132 (2016) 1–8. doi:10.1016/j.epsr.2015.11.004.

[30] H. Shaker, H. Zareipour, M. Fotuhi-Firuzabad, Reliability Modeling of Dynamic Thermal Rating, Power Delivery, IEEE Transactions on 28 (3) (2013) 1600–1609. doi:10.1109/TPWRD.2013.2252204.

[31] J. Hosek, P. Musilek, E. Lozowski, P. Pytlak, Effect of time resolution of meteorological inputs on dynamic thermal rating calculations, Generation, Transmission Distribution, IET 5 (9) (2011) 941–947. doi:10.1049/iet-gtd.2011.0039.

[32] R. Stephen, D. Douglas, G. Mirosevic, H. Argasinska, K. Bakic, S. Hoffman, J. Iglesias, F. Jakl, J. Katoh, T. Kikuta, Others, Thermal behaviour of overhead conductors, CIGRE, 2002.
URL http://www.e-cigre.org/

[33] F. Kiessling, P. Nefzger, U. Kaintzyk, J. F. Nolasco, U. Kaintzyk, Sag and tension calculations, in: Overhead Power Lines: Planning, Design, Construction, 1st Edition, Power Systems, Springer, Berlin, Heidelberg, 2003, Ch. 14, pp. 546–549. doi:10.1007/978-3-642-97879-1.

[34] CIGRE, Sag-Tension calculation methods for overhead lines - BROCHURE 324, Tech. rep. (2007).
URL http://www.e-cigre.org/

[35] A. Polevoy, Impact of Data Errors on Sag Calculation Accuracy for Overhead Transmission Line, IEEE Transactions on Power Delivery 29 (5) (2014) 2040–2045. doi:10.1109/TPWRD.2014.2325862.

[36] A. K. Deb, Line Rating Methods, in: Powerline ampacity system: theory, modeling and applications, CRC Press, 2000, Ch. 2, pp. 22–23.

[37] S. Balghouzal, J.-L. Lilien, M. El Adnani, What is the actual conductor temperature on Power Lines, Electrical and Power Engineering Frontier 2 (4) (2013) 118–129.
URL http://hdl.handle.net/2268/162834

[38] F. Van Der Heijden, R. Duin, D. De Ridder, D. M. J. Tax, Parameter Estimation, in: Classification, parameter estimation and state estimation: an engineering approach using MATLAB, John Wiley & Sons, 2004, Ch. 3, pp. 68–69.

[39] G. B. S. Allen J. Wood Bruce F. Wollenberg, Introduction to state estimation in power systems, in: Power Generation, Operation and Control, 3rd Edition, Wiley-Interscience, 2013, Ch. 9, pp. 410–417.

[40] A. Michiorri, H.-M. Nguyen, S. Alessandrini, J. B. Bremnes, S. Dierer, E. Ferrero, B.-E. Nygaard, P. Pinson, N. Thomaidis, S. Uski, Forecasting for dynamic line rating, Renewable and Sustainable Energy Reviews 52 (2015) 1713–1730. doi:10.1016/j.rser.2015.07.134.

[41] S. M. Mahajan, U. M. Singareddy, A Real-Time Conductor Sag Measurement System Using a Differential GPS, Power Delivery, IEEE Transactions on 27 (2) (2012) 475–480. doi:10.1109/TPWRD.2011.2181963.

[42] C. W. G. B2.12, I. C. on Large Electric Systems, Guide for Selection of Weather Parameters for Bare Overhead Conductor Ratings, CIGRE, 2006.
URL http://www.e-cigre.org/